Received: May 29, 2017
Revised: June 26, 2017
Accepted: June 27, 2017

Structural Properties of Copper Zinc Oxide Nanoparticles prepared from Solid State Reaction

W. Phoohinkong, T. Foophow, T. Sukonket

Faculty of Science and Technology, Suan Dusit University, Bangkok, 10700, Thailand

Abstract

Local structure of copper zinc oxide nanoparticles synthesized from single step solid state synthesis was investigated. The phase structure of the copper zinc oxide nanopowder product was confirmed by X-ray powder diffraction (XRD). The particle size and morphology were investigated by field emission scanning electron microscopy (FESEM) and transmission electron microscopy (TEM). Short range crystal fine structure was investigated by X-ray absorption spectroscopy (XAS). The result demonstrates that the Cu atom probably substitutes in Zn site of ZnO wurtzite host. The second phase of CuO nanocluster was presented in the Cu doped ZnO structure as the Cu concentration is in the range of 10 and 50 %mole. The radial distribution functions in short range order from Zn atom, points to a high concentration of O and Zn vacancies in all samples which correlates with the distortion of local symmetry ZnO cluster compared with ZnO standard. A higher disorder corresponds to the interpreted XRD result in terms of crystallinity degree which is likely originated by a disorder of surface and interface effect. The prepared sample with 1.0 mol% Cu shows smaller particle size with highly distorted ZnO cluster and high O and Zn vacancies. These copper zinc oxide nanoparticles with high active surface and high phase interface could be feasibly promising material in many applications.

1. Introduction

Copper-doped zinc oxide nanoparticles and copper zinc oxide nanocomposites are well known for various fields of application such as highly selective catalysts [1-6], electronics (spintronics) and optoelectronics for dilute magnetic semiconductors (DMSs) [7,8], sensors [9-11], energy conversion [12], and solar cells [13]. Unique properties for specific application highly depend on active site from surface structure, morphology, interface, composition, chemical doping concentration and preparation methods which generate the appropriate active site cluster on particles. Numerous synthesis techniques for Cu-Zn-O compounds with different nanostructures (nanorods, nanoparticles, nanowires and nanocomposite) such as atomic layer deposition (ALD) [1], co-precipitation [3], reflux method [4], hydrothermal [6, 11], sol–gel process [7], thermal decomposition [8], solvothermal [9] biological template [10] have been reported. The nature of the active sites that originate from electronic structure and surface terminal lattice structure requires further deep investigation. These information corresponds to the local structure information of atomic level cluster in the short range order crystal which can be obtained by X-ray absorption spectroscopy study [5, 14-23].

Since results from XRD, SEM and TEM may be insufficient for any feature information which could be assigned to Cu phase, state and local structure, especially when the interesting CuO and ZnO cluster are presented in nanocrystal cluster and/or amorphous-like structures at surface, interface or lattice defect, many researches have employed useful tool of XAS technique to accurately characterize and study the synthesized copper zinc oxide compounds. Bjerne S. Clawen *et al.* [15] used XRD, TEM and XAS technique to elucidate local

*Corresponding Author E-mail:*p_veerachon@hotmail.com

environment structure of binary Cu-Zn methanol catalysts and found somewhat difference of Cu in well-crystallized of bulk CuO. Evgeny Kleymenov *et al.* [17] employed XAS and EXAFS data for studying structure of the active catalyst Cu and ZnO predominantly of methanol synthesis and identifying the intermediate state and local structure change of the catalyst during methanol formation. Sabina M. Hatch *et al.* [18] used extended x-ray absorption fine structure (EXAFS) analysis to investigate the site-specific feature of deep-level photoluminescence in ZnO nanorods. The obtained information provided that the different emission energy primarily originated from the nanorod was linked to site-specific crystal structures which was different between nanorod surface defects and disorder crystal structure on Zn sites. Local structure information revealed by XAS study is also an obvious evidence to understand relevant properties [19] of copper zinc oxide such as the improvement of dielectric property due to the introduction of Cu ions occupying in Zn site of ZnO host and induced local electric dipoles by Cu-O bond combining with the presence of oxygen vacancies that facilitates the ferroelectric domain boundary movement[21]. The magnetic moments of copper zinc oxide typically display paramagnetic property according to the presence of Cu impurities substituting in Zn site in the wurtzite lattice of ZnO that can be confirmed by XRD and x-ray XAS technique [23].

In this study, we investigate in the structure in a complex solid matrix of copper zinc oxide nanoparticles synthesized by a solid state reaction route with different Cu concentrations in the starting precursor designated at 0.1, 1.0, 10 and 50mol%. The prepared copper zinc acetate starting reactant was studied by Raman spectroscopy. The detailed information of synthesized copper zinc oxide compounds was studied by XRD, FESEM, TEM and local structure was investigated by EXAFS.

2. Procedure

2.1. Preparation of copper zinc acetate precursors

The starting copper zinc acetate precursor series with various copper acetate concentration were prepared using the methods as in the previous work [24]. Copper zinc acetate precursor was prepared from mixtures of CuO and ZnO for 0.1, 1.0, 10, 50 mol% dissolved with glacial acetic acid followed by deionized water to obtain the solution of copper zinc acetate, then crystallization to obtain acetate salt from solutions. Copper zinc acetate salt prepared from Cu 0.1, 1.0, 10 and 50 mol% are assigned to CZO Ac-Cu0.10, CZO Ac-Cu1.0, CZO Ac-Cu10 and CZO Ac-Cu50, respectively.

2.2. Synthesis of copper zinc oxide nanopartic

Copper zinc oxide nanoparticles were synthesized by conventional solid state reaction method described in our previous article [24]. Briefly, divalent metal copper zinc acetates salts were mixed with sodium hydroxide powder then was ground for 15 min. The final product was washed with distilled water then dried at 80°C for 24 h. Copper zinc oxide nanoparticles derived from 0.1, 1.0, 10 and 50 mol% of Cu in acetate precursor are ascribed as CZO-Cu0.10, CZO-Cu1.0, CZO-Cu10 and CZO-Cu50, respectively.

2.3. Characterization

Ligand coordination character of the starting copper zinc acetate precursor powders was identified by Raman spectroscopy with 530 nm laser source. The XRD of copper zinc oxide

product was recorded using XRD PANalytical X'PertPro using Cu-K_α radiation operated at 40 kV 30 mA. FE-SEM images were obtained from FE-SEM MODEL: HITACHI – S4700 and for higher resolution were observed by TEM Philips–Tecnai 12. The Zn and Cu K-edge absorption information spectra data was obtained using X-ray absorption spectroscopy in transmission mode and tuning the photon energy by Ge (220) double-crystal monochromator. Experiment of EXAFS spectroscopy using synchrotron radiation was performed at station at beam line 8 of the Synchrotron Light Research Institute (SLRI) (Public Organization), Nakhon Ratchasima, Thailand. EXAFS processing for transforming from energy space to momentum (k) space and Fourier transform (FT) from k-space to real R-space as a radial distribution functions was performed using the ATHENA and Artemis software package.

3. Results and Discussion

Figure 1 shows Raman spectra of as-prepared copper zinc acetate precursors relating to free and bidentate acetate ligand having symmetry of C2v and 15 peaks of 5A, + A2 + 5Bl + 4B2 with all are Raman active [25]. The Raman in 680–1,000 cm^{-1} region is information for the study of solid acetates salt possessing high scattering intensity. The Raman spectra at 693 and 950 cm^{-1} ascribe to the O–C–O deformation region of acetates bending mode and the C–C symmetric stretching vibration on the acetate ion [25-28], respectively.

There are characteristic spectra of acetate salt complex supported by the addition of methyl H–C–H coordinated acetate deformation and rocking vibration peak around 1360 cm^{-1}. The peaks of C=O stretching vibrations are in the regime of 1200 – 1650 cm^{-1} attributing to carboxylic acids formed to acetate salts and the C=O and C–O bonds act as equivalent of two C---O (1.5 bonds order) interacting as in-phase and out-of-phase vibrations in two band of the symmetric stretch vibration mode (V_s(COO−)) and antisymmetric stretching vibration mode (V_{as}(COO−)). The complex bands of the stretching C=O vibrations region are traditionally used to evaluate the type of acetate ligand coordination with metal ion of acetate salt. The various coordination types of acetate salt identified by the different values between v_s and v_{as} at which the symmetric C-O stretching vibration mode is V_s(C-O) and the antisymmetric C=O stretch vibration mode is V_{as}(C=O). The typical values are; $v_s > 1415$ cm^{-1} and $v_{as} < 1560$ cm^{-1} for bidentate acetate ligand, v_s around 1415 cm^{-1} and v_{as} around 1560 cm^{-1} for bridged acetate ligand, $v_s < 1415$ cm^{-1} and $v_{as} > 1560$ cm^{-1} for monodentate acetate ligand as shown as the inset of Figure 1. Unfortunately, by equipment limitation, we are unable to use symmetry to identify distinct difference between v_s and v_{as} (Δv values) from this data set and to examine the type of ligand bonding in the prepared acetate salt sample [25-28]. Moreover, the main Raman spectrum located at 2940 cm^{-1} and 3037 cm^{-1} exhibit clearly sharp, intense peaks assigning to characteristic of symmetric and antisymmetric C–H stretching mode vibrations in the methyl group. These results from Raman study of the obtained copper zinc acetates clearly indicate purity acetate salts without the signal of impurity of starting ZnO and CuO which should exhibit signal at 633 to 665 cm^{-1} [29, 30], or contaminant by product such as sodium acetate which should exhibits characteristic peaks at 910-935, 1009-1017, 1100 and 1342-1350 cm^{-1} [31-33].

Fig. 2 shows the typical XRD patterns of as-synthesized copper zinc oxide nanoparticles obtained from different starting copper contents. All predominant reflection peaks in this pattern are found to nicely match with ZnO zincite with hexagonal geometry [JCPDF # 071-6424]. The other reflection peaks corresponding to CuO related secondary phase are found in copper oxide doped zinc oxide CZO -Cu10 and CZO -Cu50 samples, which may be attributed

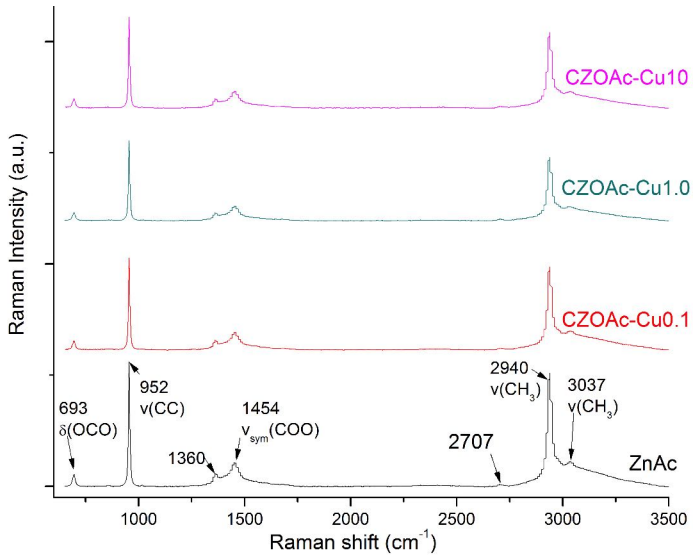

Fig. 1. The Raman spectra of the prepared copper zinc acetate.

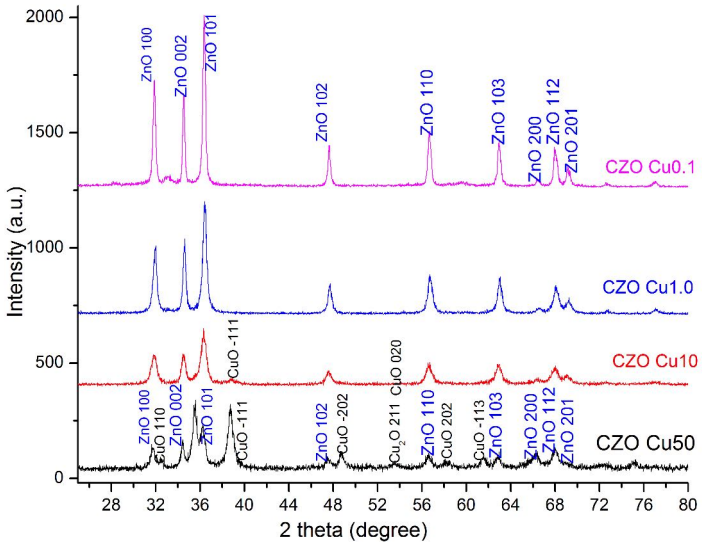

Fig. 2. XRD patterns of as-synthesized copper zinc oxide nanoparticles obtained from 0.1, 1.0, 10.0 and 50.0 mol% Cu in the starting precursor.

to the incorporation of CuO nanocrystal cluster into the ZnO lattice. This feature indicates that there is significant Cu atom tending to be doped in ZnO host in all Cu concentration, even at high Cu concentration up to 10mol% in precursor. The CuO peaks pattern dominantly appear for CZO -Cu50 sample while the ZnO peaks show broadening character and weaker intensity, which can be explained by the smaller crystalline size of ZnO when copper content increases.

FESEM images of copper zinc oxide nanoparticles prepared with different Cu contents are presented in Fig. 3(a) – 3(d) for CZO - Cu0.10, CZO - Cu1.0, CZO - Cu10 and CZO - Cu50,

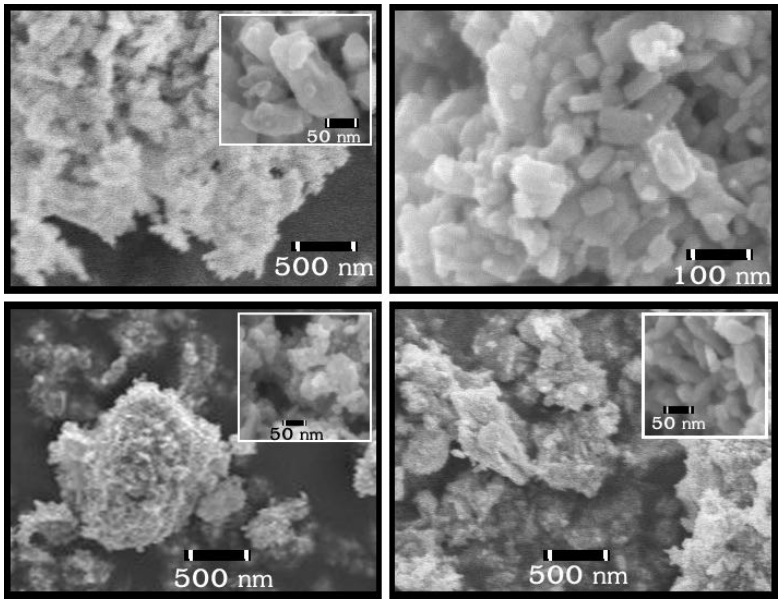

Fig. 3. FESEM images of copper zinc oxide nanoparticles prepared from different Cu concentration acetate salts (a) CZO –Cu0.1, (b) CZO –Cu1.0, (c) CZO –Cu10 and (d) CZO – Cu50.

respectively. FESEM images show different particle size and morphology as the copper concentration is varied. CZO -Cu0.1 (Fig. 3a) exhibits the main particle with nano-dimensional sizes in the range of 50 – 200 nm with a small proportion of smaller particle. CZO -Cu1.0 in Fig. 3b illustrates particle growth with rod-like shape in the particle dimension of around 30 and 100 nm. CZO -Cu10 image displays smaller particle with particle size of around 20 nm while CZO -Cu10 presents larger grain size with particle dimension of around 25 and 100 nm.

The typical morphologies from TEM image are shown in Fig. 4a–d. According with FESEM image results, the corresponding higher resolution images show more clearly in particle size and shape. TEM image of CZO -Cu0.1 in Fig. 4a reveals that the nanopowder samples are composed of the rod-like particles with size around 200 nm in diameter and aggregated cluster of small spherical primary particles with size around 5 nm. As seen in Fig. 4b, CZO -Cu1.0 TEM image indicates the rod-like structures with hexagonal shape with their size of about 25-50 nm. The CZO -Cu10 samples show small nodular particles with size around 10 nm as observed in Fig. 4c. TEM image of the CZO -Cu50 in Fig. 4d reveals the two ranges of particle size and shape; 5-25 nm nodular structure and rod-like shape with 30-50 nm in diameter. The typical average particle grain sizes in FESEM and TEM images are well agreed to the trend of crystalline size interpreted by FWHM of XRD results.

Synchrotron XAS technique was performed to further examine in the local atomic structure of the copper zinc oxide nanoparticles samples for clarifying the small cluster which may in form amorphous-like structures, existence of a secondary Cu phase in the ZnO structure and local structure of Cu dopant atom in the environment of ZnO host. The normalized Zn and Cu K-edge XANES spectra for the bulk ZnO standard and all prepared copper zinc oxide samples were transformed to EXAFS oscillation patterns of $k^2\chi(k)$ as shown

in Fig. 5a. The corresponding Fourier transforms (FT) of EXAFS oscillation spectra from K-space in to R-space in terms of distances from the Zn atom are accordingly shown in Fig. 5b. Overall oscillation spectra and Fourier transforms shape results as function of Cu concentration indicate that the strong peaks pattern of prepared samples are in analogous agreement to Zn K-edge EXAFS signal of bulk wurtzite ZnO. This well-evidence suggests that Cu^{2+} ions for all doping concentrations are largely incorporated into Zn sites in the host wurtzite ZnO lattice fingerprinting crystallographic [19, 34, 36]. The position of the FT peaks at Zn K-edge is quite similar to bulk ZnO for all samples with each other (without change in position displayed in overlay patterns in the bottom of Fig. 5b.) This characteristic exhibits most ordered well crystalline of ZnO wurtzite for the next-nearest-neighbor (NNN) shell with in the particle size in the nano range [36] but the peaks are slightly distinct in magnitudes of the FT pattern. Therefore, these results indicate the existence of disordered environment around Zn atom of prepared samples, which mean that the Cu concentration has a significant effect to local crystallinity around Zn atom.

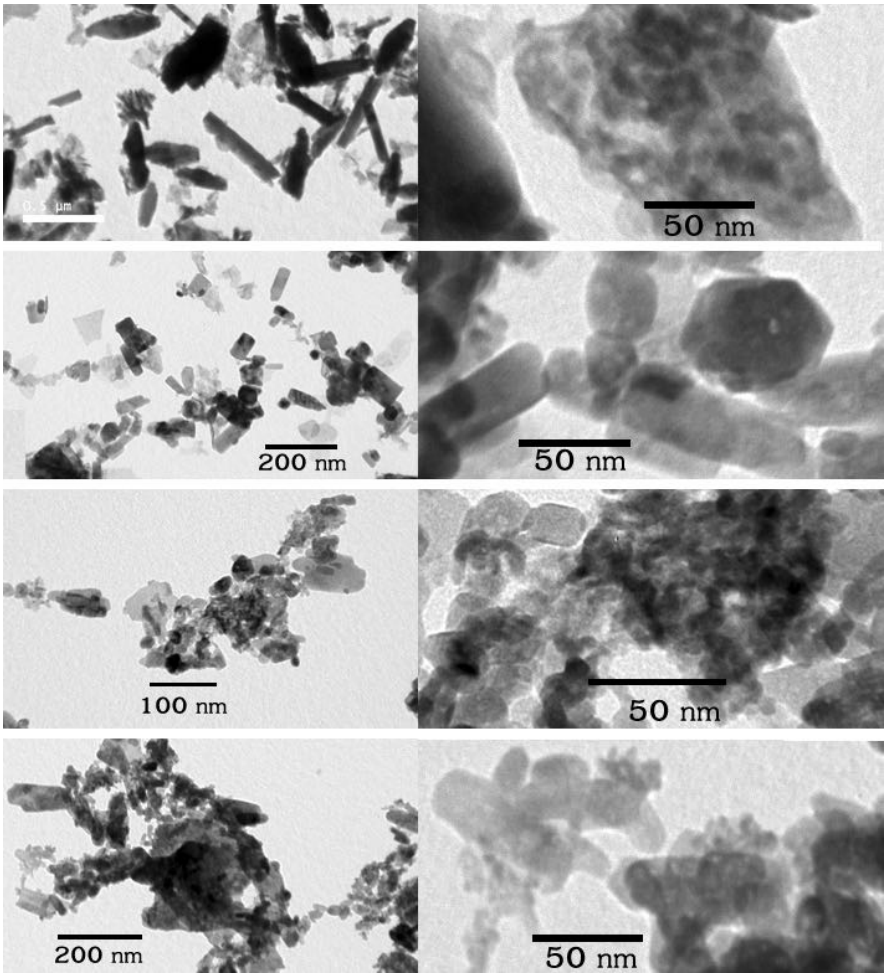

Fig. 4. TEM images of copper zinc oxide nanoparticles (a) CZO –Cu0.1, (b) CZO –Cu1.0, (c) CZO –Cu10 and (d) CZO –Cu50.

The first peak in the Zn K-edge FT($\chi(k)*k^2$) as noticed in Fig. 5b is attributed to Zn surrounded by first shell of nearest-neighbor (NN) oxygen atom in a distorted tetrahedral coordination and the second peak (NNN) is typically associated to the first Zn-Zn distances shell (and small proportion of Cu in Cu-doped ZnO matrix) in ZnO [5, 19-21]. The first oxygen shell (Zn-O1) shell exhibits a strong intensity for CZO –Cu1.0 to CZO –Cu50 compared to bulk ZnO standard. CZO –Cu0.1 FT pattern reveals a decreased peak intensity of the first Zn-O shell that disorders will exist in the Zn–O pairs bond length compared with the bulk ZnO counterpart due to the decrease in coordination number (N) of O and the increase in the Debye-Waller (DW) factors [19, 35]. This manner implies that the structure is incorporated with oxygen vacancies. It is assumed that only few lattice cluster layers from the boundary are disorder of Zn–O local symmetry, effectively affected by the unsaturated coordination bonds at the surface/interface boundary of nanoparticles or nanocrystals. However, XRD results and TEM images indicate higher crystallinity with greater particle size. This contrary may relate to the disorder in CZO –Cu0.1 sample induced by oxygen vacancies.

As a function of Cu doping concentration, it is observed that the second shell of FT at Zn K-edge of all Cu doping concentration significantly decreases in its peak amplitude comparing to bulk ZnO standard counterpart. CZO –Cu0.1 has the lowest peak intensity while the values of rest samples are insignificantly different. Therefore, the decrease in atomic distance order for second coordination shell can be attributed to lattice disorder by surface effect of nanoparticles and predominately ascribes to higher concentration of Zn vacancies especially in CZO –Cu0.1 sample [19-21, 35]. FT peak around 3.5 to 4.5 Å different from bulk ZnO for the all Cu-doped samples provides further evidence for Cu dopant presented in the long range ZnO crystalline structure around Zn atom.

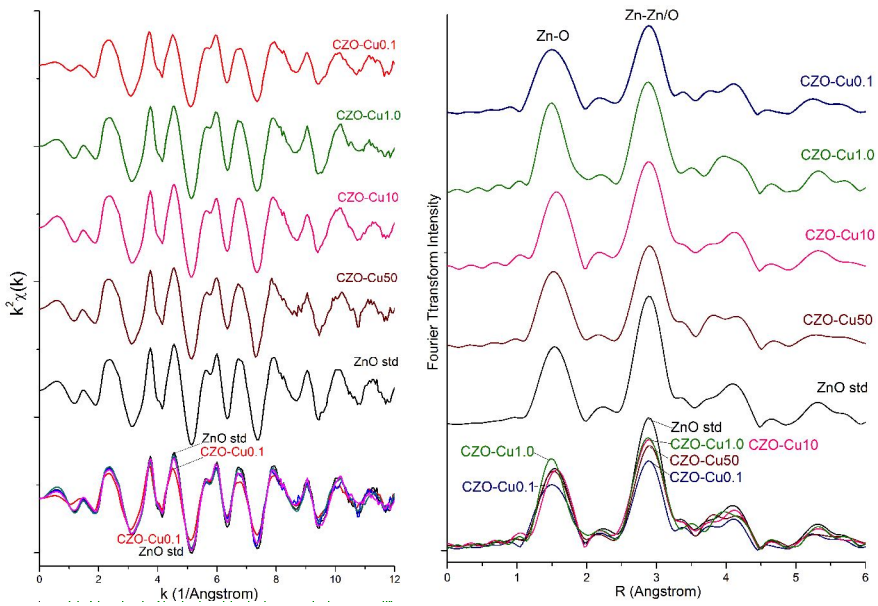

Fig. 5. Zn K-edge EXAFS k^2 weighted oscillation spectra (a) and corresponding fourier transforms (b).

EXAFS signals $k^2\chi(k)$ oscillations at the Cu K-edge for the copper zinc oxide nanoparticles; CZO -Cu1.0, CZO -Cu10 and CZO -Cu50 samples compared with the reference CuO and Cu_2O standard materials are shown in Fig. 6. There is no data for the CZO –Cu0.1sample due to XAS transmission mode limit in very low atom concentration (Fig. 6a). The corresponding fourier transforms to the mean radial distribution functions are displayed in Fig. 6b. Two major peaks can be observed in Cu K-edge FT($\chi(k)*k^2$) pattern. The first peak of neighbor atom attributes to an Cu-O bond length in a square-planar coordination shell in bulk tenorite CuO and the second shell corresponds to Cu to metal (Zn/Cu) distance [22, 23]. Cu K-edge EXAFS oscillation patterns and corresponding FT profile of CZO –Cu10 and CZO -Cu50 samples show quite different oscillations signal from CuO standard, indicating the considerable difference in local environment of Cu atom in both samples. Cu^{2+} ions in CZO –Cu10 and CZO -Cu50 samples are also likely in CuO bond distance in the copper zinc oxide samples, especially for CZO -Cu50 samples showing a feature that is close to the bulk CuO structure. This feature could be assignd to the CuO nanocluster corresponding to the presence of second phase. However, all samples are also composed of Cu^{2+} that occupies Zn^{2+} in ZnO without significant distortions in the ZnO host [21, 37] that agrees well with the results from EXAFS signals at the Zn K-edge. The third weak FT peak and long range pattern could be attributed to long range coordination compared with bulk CuO standard confirming the existence of CuO nanocluster in CZO –Cu10 and CZO -Cu50 samples and presence in a square planar coordination of monoclinic tenorite CuO. The first and second coordination shell maximum of CZO -Cu1.0 in the radial distribution functions pattern (Fig. 6b) are significantly shorter than the Cu-O and Cu-Cu distance in bulk CuO tenorite, which indicates that local environment around Cu atom may exist in the tetrahedron coordination environment of hexagonal wurtzite [22, 23].

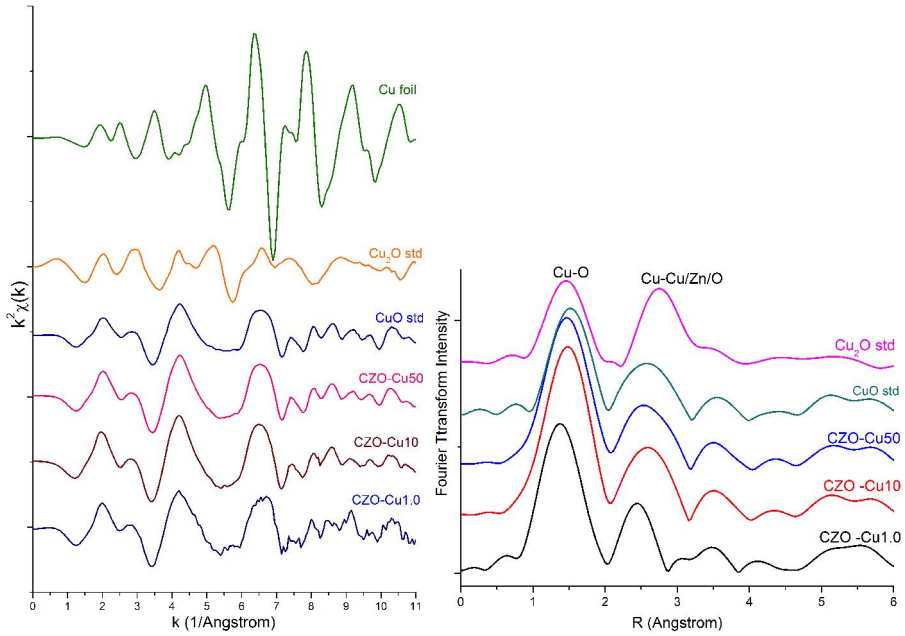

Fig. 6. Cu K-edge EXAFS k^2 weighted oscillation functions on wave vector k (a) and is shown in the mean radial distribution functions (b).

4. Conclusion

The structural properties of copper zinc oxide nanoparticles with different Cu concentrations prepared by solid state reaction exhibit multiphase amorphousity, nanocrystalline structure and multi structural Cu local environment at different Cu concentration. At low Cu concentration of 0.1 and 1.0 mol% precursor, Cu^{2+} ions may occupy in Zn sites in the wurtzite environment of the ZnO host meanwhile higher Cu concentration at 10 and 50 mol% leads to the existence of square planar coordination of monoclinic environment of CuO nanocrystal second phase. These observations of local structure are in good agreement with the XRD data. The highest O and Zn vacancies are assigned to the sample obtained from 1.0 mol% Cu precursor. As a result, the high active site copper zinc oxide nanoparticles may be a feasible promising high active material in many applications.

Acknowledgements

The authors would like to thank the beam line station 8 (BL8) of Synchrotron Light Research Institute (Public Organization) for X-ray beam time and their technical support.

References

[1] W. Wang, F. Wu, Y. Myung, D.M. Niedzwiedzki, H.S. Im, J.H. Park, P. Banerjee and P. Biswas, Surface Engineered CuO Nanowires with ZnO Islands for CO_2 Photoreduction, *ACS Appl. Mater. Interfaces* 7 (2015), 5685–5692.

[2] X. Wang, K. Ma, L. Guo, Y. Tian, Q. Cheng, X. Bai, J. Huang, T. Ding, X. Li, Cu/ZnO/SiO_2 catalyst synthesized by reduction of ZnO-modified copper phyllosilicate for dimethyl ether steam reforming, *Applied Catalysis A: General* 540 (2017), 37-46.

[3] I. Kim, G. Lee, H. Jeong, J.H. Park and J.C. Jung, Bifunctionality of Cu/ZnO catalysts for alcohol-assisted low-temperature methanol synthesis from syngas: Effect of copper content, *Journal of Energy Chemistry*, In Press, Corrected Proof, Available online 20 February 2017.

[4] A.N. Kadam, T.G. Kim, D.S. Shin, K.M. Garadkar and J. Park, Morphological evolution of Cu doped ZnO for enhancement of photocatalytic activity, *Journal of Alloys and Compounds* 710 (2017), 102-113.

[5] V.D. Berg, W.E. Maurits, P. Sebastian, O.P. Tkachenko, K. Kolja, M. Martin and G. Wolfgang, Dynamical Changes in the Cu–ZnO_x Interaction Observed in a Model Methanol Synthesis Catalyst, *Catalysis Letters* 128 (2009), 49-56.

[6] J. Zhang, T. Chen, J. Yu, C. Liu, Z. Yang, H. Lu, F. Yin, J. Gao, Q. Liu, X. Zhang and Y. Tu, Enhanced photocatalytic activity of flowerlike CuO–ZnO nanocomposites synthesized by one-step hydrothermal method, *Sci: Mater Electron* 27 (2016), 10667.

[7] H. Liu, L. Fei, H. Liu, J. Lang, J. Yang, Y. Liu, M. Gao, X. Liu, X. Cheng and M. Wei, Effects of annealing atmosphere on structure, optical and magnetic properties of $Zn_{0.95}Cu_{0.02}Cr_{0.03}O$ diluted magnetic semiconductors, *Journal of Alloys and Compounds* 587 (2014), 222-226.

[8] K. Noipa, S. Rujirawat, R. Yimnirun, V. Promarak and S. Maensiri, Synthesis, structural, optical and magnetic properties of Cu-doped ZnO nanorods prepared by a simple direct thermal decomposition route, *Appl. Phys. A* 117 (2014), 927.

[9] S. Park, S. Kim, H. Kheel, S.K. Hyun, C. Jin and C. Lee, Enhanced H_2S gas sensing performance of networked CuO-ZnO composite nanoparticle sensor, *Materials Research Bulletin* 82 (2016) 130-135.

[10] M. Maruthupandy, Y. Zuo, J.S. Chen, J.M. Song, H.L. Niu, C.J. Mao, S.Y. Zhang and Y.H. Shen, Synthesis of metal oxide nanoparticles (CuO and ZnO NPs) via biological template and their optical sensor applications, *Applied Surface Science* 397 (2017), 167-174.

[11] M.M. Rahman, A. Jamal, S.B. Khan and M. Faisal, CuO Codoped ZnO Based Nanostructured Materials for Sensitive Chemical Sensor Applications, *ACS Appl. Mater. Interfaces* 3 (2011), 1346–1351.

[12] A. Dhara, B. Show, A. Baral, S. Chabri, A. Sinha, N.R. Bandyopadhyay and N. Mukherjee, Core-shell CuO-ZnO p-n heterojunction with high specific surface area for enhanced photoelectrochemical (PEC) energy conversion, *Solar Energy* 136 (2016), 327-332.

[13] M.H. Habibi, B. Karimi, M. Zendehdel, M. Habibi, Fabrication, characterization of two nano-composite CuO–ZnO working electrodes for dye-sensitized solar cell, *Spectrochimica Acta Part A: Molecular and Biomolecular Spectroscopy* 116 (2013), 374-380.

[14] S.V. Didziulis, K.D. Butcher, S.L. Cohen and E.I. Solomon, Chemistry of Copper Overlayers on Zinc Oxide Single-Crystal surfaces: model active sites for copper/zinc oxide methanol synthesis catalysts, *J. Am. Chem. Soc*. 111 (1989), 7110-7123.

[15] B.S. Clausen, B. Lengeler and B.S. Rasmussen, X-ray absorption spectroscopy study of copper-based methanol catalysts. 1. Calcined state, *J. Phys. Chem*. 89 (1985), 2319-2324.

[16] K. Tohji, Y. Udagawa, T. Mizushima and A. Ueno, The structure of the copper/zinc oxide catalyst by an in-situ EXAFS study, *J. Phys. Chem*. 89 (1985), 5671-5676.

[17] E. Kleymenov, J. Sa, J. Abu-Dahrieh, D. Rooney, J.A.V. Bokhoven, E. Troussard, J. Szlachetko, O.V. Safonova and M. Nachtegaal, Structure of the methanol synthesis catalyst determined by in situ HERFD XAS and EXAFS, *Catal. Sci. Technol*. 2 (2012), 373-378.

[18] S. M. Hatch, A. Sapelkin, G. Cibin, R. Taylor, A. Dent, J. Briscoe and S. Dunn, Investigating the source of deep-level photoluminescence in ZnO nanorods using optically detected x-ray absorption spectroscopy, *Journal of Applied Physics,* 114 (2013), 153517.

[19] P. Satyarthi, S. Ghosh, Y. Wang, S. Zhou, D. Bürger, I. Skorupa, H. Schmidt, L. Olivi and P. Srivastava, Direct evidence of defect coordination and magnetic interaction in local structure of wurtzite type $Zn_{1-x}Co_xO$ thin films, *Journal of Alloys and Compounds* 670 (2016), 113-122.

[20] D. Gallach, A. Muñoz-Noval, V. Torres-Costa and M. Manso-Silván, Luminescence and fine structure correlation in ZnO permeated porous silicon nanocomposites, *Phys. Chem. Chem. Phys*. 17 (2015), 20597-20604.

[21] H. Liu, Y. Wang, J. Wu, G. Zhang and Y. Yan, Oxygen vacancy assisted multiferroic property of Cu doped ZnO film, *Phys. Chem. Chem. Phys*. 17 (2015), 9098-105.

[22] V.V. Pelipenko, D.I. Kochubey, AA. Khassin and T.M. Yurieva, Evolution of the Cu/ZnO methanol synthesis catalyst during its reduction and re-oxidation, *React Kinet. Catal. Lett*. 86 (2005), 307–314.

[23] P.S Vachhani, G. Dalba, R.K. Ramamoorthy, F. Rocca, O. Šipr and A.K Bhatnagar, Cu doped ZnO pellets: study of structure and Cu specific magnetic properties, *Journal of Physics: Condensed Matter*. 24 (2012), 506001.

[24] W. Phoohinkong, T. Foophow and W. Pecharapa, Synthesis and characterization of copper zinc oxide nanoparticles obtained via metathesis process, *Advances in Natural Sciences: Nanoscience and Nanotechnology*, (In Press, Corrected Proof.)
[25] M.M. Yang, D.A. Crerar and D.E. Irish, A Raman spectroscopic study of lead and zinc acetate complexes in hydrothermal solutions, *Geochimica et Cosmochimica Acta.* 53 (1989), 319-326.
[26] F. Quilès and A. Burneau, Infrared and Raman spectra of alkaline-earth and copper(II) acetates in aqueous solutions, *Vibrational Spectroscopy* 16 (1998), 105-117.
[27] A. Musumeci and R.L. Frost, A spectroscopic and thermoanalytical study of the mineral hoganite, *Spectrochimica Acta Part A: Molecular and Biomolecular Spectroscopy* 67, (2007), 48-57.
[28] T. Ishioka, Y. Shibata, M. Takahashi and I. Kanesaka, Vibrational spectra and structures of zinc carboxylates II. Anhydrous zinc acetate and zinc stearate, *Spectrochimica Acta Part A: Molecular and Biomolecular Spectroscopy* 54 (1998), 1811-1818.
[29] J.X. Wang, X.W. Sun, Y. Yang, K.K.A. Kyaw, X.Y. Huang, J.Z. Yin, J. Wei and H.V. Demir, Free-standing ZnO–CuO composite nanowire array films and their gas sensing properties, *Nanotechnology* 22 (2011), 325704.
[30] S. Kuriakose, D.K. Avasthi, S. Mohapatra, Effects of swift heavy ion irradiation on structural, optical and photocatalytic properties of ZnO–CuO nanocomposites prepared by carbothermal evaporation method, *Beilstein J Nanotechnol*. 2015, 6, 928–937.
[31] V.M. Padmanabhan, Raman spectra of crystalline acetates (sodium, magnesium and barium), Proceedings of the Indian Academy of Sciences - Section A. 37 (1953), 401-404.
[32] H. Noma, Y. Miwa, I. Yokoyama and K Machida, Infrared and Raman intensity parameters of sodium acetate and their intensity distributions, *Journal of Molecular Structure* 242 (1991), 207-219
[33] R.L Frost and J.T Kloprogge, Raman spectroscopy of the acetates of sodium, potassium and magnesium at liquid nitrogen temperature, *Journal of Molecular Structure* 526 (2000), 131-141.
[34] F.A. Akgül, Influence of Ti doping on ZnO nanocomposites: Synthesis and structural characterization, *Composites Part B: Engineering* 91 (2016), 589-594.
[35] S.W. Han and H.J. Yoo, Orientation-dependent x-ray absorption fine structure of ZnO nanorods, *Appl. Phys. Lett*. 86 (2005), 021917.
[36] C.C. Yang and S.Y. Chen, Physical characterization of ZnO nanorods grown on Si from aqueous solution and annealed at various atmospheres*, J. Vac. Sci. Technol. B* 23, (2005), 2347-2350.
[37] O. Šipr, J. Vackář, P.S. Vachhani, R.K. Ramamoorthy, G. Dalba, A.K. Bhatnagar and F Rocca, Local structure and magnetism of Cu-doped ZnO via Cu K-edge XAS and XMCD: theory and experiment, *J. Phys.: Conf. Ser.* 430 (2013), 012128.